MCP-PMT development at Argonne for particle identification

J. Xie,[a,1] **M. Chiu,**[b] **E. May,**[c] **Z.-E. Meziani,**[a] **S. Nelson**[d] **and R. Wagner**[c]

[a] *Physics Division, Argonne National Laboratory,*
  9700 S. Cass Ave., Lemont, IL 60439, U.S.A.

[b] *Physics Department, Brookhaven National Laboratory,*
  PO Box 5000, Upton, NY 11973, U.S.A.

[c] *High Energy Physics Division, Argonne National Laboratory,*
  9700 S. Cass Ave., Lemont, IL 60439, U.S.A.

[d] *Department of Physics, Florida A&M University,*
  1601 S. Martin Luther King Jr. Blvd., Tallahassee, FL 32307, U.S.A.

  E-mail: jxie@anl.gov

Abstract: The proposed high-energy high-luminosity polarized Electron-Ion Collider (EIC) demands excellent particle identification over a wide range of particles momenta to achieve the best separation between signal and background particles. Various Cherenkov imaging detector sub-systems are being considered in EIC detector concepts for hadron identification for particles momenta up to 50 GeV/c. One important challenge in this case is to provide a reliable highly pixelated photosensor working in the high radiation and high magnetic field environment. The recently commercialized Large Area Picosecond Photo-Detector (LAPPD) provides a promising low-cost photosensor solution for the various EIC Cherenkov imaging sub-systems. Optimization of the phtosensor design for high magnetic field tolerance, precision timing resolution, and pixelated readout was performed at Argonne National Laboratory with $6 \times 6 \, \text{cm}^2$ microchannel plate photomultipliers. The techniques and optimized design parameters would be transferrable to industrial partners for low-cost LAPPD production to achieve the demonstrated performance.

---

[1]Corresponding author.

https://doi.org/10.1088/1748-0221/15/04/C04038

Contents

1 Introduction

The Electron-Ion Collider (EIC) [1] was recommended as the highest priority for new facility construction following the completion of the Facility for Rare Isotope Beams (FRIB) in the 2015 long-range plan for Nuclear Physics [2]. Following the recommendation, a group of committee members from the National Academies conducted a 14-months study to examine the scientific importance of an EIC, as well as the international implications of building a domestic EIC facility, and concluded that the science that could be addressed by an EIC is compelling and would provide long-elusive answers on the nature of matter [3].

Identification of hadrons in the final state is essential for key EIC measurements, including 3D imaging of the nucleon in momentum space through semi-inclusive deep inelastic scattering (SIDIS) and open charm production (with decays of D-mesons into kaons). The physics of interest requires hadron particles detection and identification (π/K/p separation of better than 3 sigma) over the full angular range and particle momentum reach up to 50 GeV/c: π/K/p identification in the central barrel up to $\sim$ 7 GeV/c, in the electron-going endcap up to $\sim$ 10 GeV/c, and in the hadron-going endcap up to $\sim$ 50 GeV/c. A suite of detector technologies that can address the specific challenges (in terms of momentum coverage, available space, etc. . .) encountered in various ranges of rapidity are required to satisfy the particle identification (PID) requirements [4]. Considering the particle kinematics coverage, spatial constraints and the relative cost, different detectors based on Cherenkov radiation have been proposed, a dual-radiator Ring Imaging Cherenkov (dRICH) detector in the hadron endcap, a compact detector based on the Detection of Internally Reflected Cherenkov light (DIRC) approach in the central barrel, and a compact aerogel modular RICH (mRICH) detector in the electron-going endcap. In principle, a gas-only RICH can be built within the same geometry as a dRICH, changing

the overall shape of the RICH detector from a cylinder to a cone. Depending on the overall layout of the detector, the gas-only RICH may be easier to integrate with the other sub-systems.

The specific requirements that the DIRC and the various RICH detectors must fulfil within the scope of the EIC detectors pose unique constraints on photosensors and electronics performance, different from any previous DIRC and/or RICH implementation. The EIC PID consortium (eRD14 Collaboration) has been formed to identify and develop PID detectors using ring imaging Cherenkov (RICH) techniques for the futureEIC experiments in a broad kinematic coverage. Table 1 below lists the minimum requirements on high-performance DIRC, mRICH, and dRICH photosensors. More specifically, a small pixel size of 2–3 mm and a tolerance to magnetic fields in the range of 1.5–3 T are unique constraints. Therefore, developing reliable low-cost highly pixelated photosensors working in high radiation and high magnetic-field environment becomes a key challenge for the EIC particle identification [5].
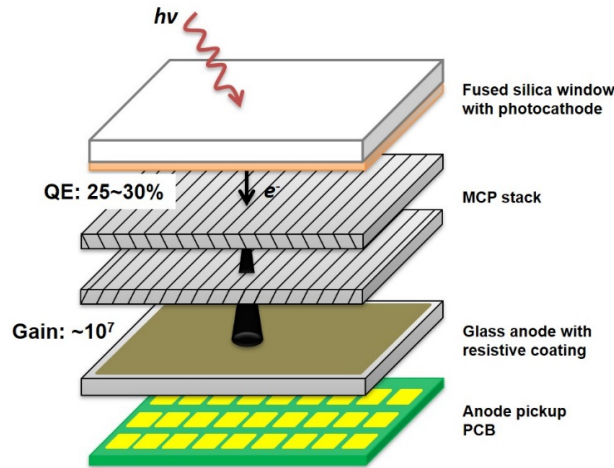
Table 1. A list of performance requirements of the photosensors for the EIC PID Cherenkov detectors.

Parameter	DIRC	mRICH, dRICH
Gain	$\sim 10^6$	$\sim 10^6$
Timing Resolution	≤ 100 ps	≤ 800 ps
Pixel Size	2–3 mm	≤ 3 mm
Dark Noise	$\leq 1\,\text{kHz/cm}^2$	$\leq 5\,\text{MHz/cm}^2$
Radiation Hardness	Yes	Yes
Single-photon mode operation	Yes	Yes
Magnetic-field tolerance	Yes (1.5–3 T)	Yes (1.5–3 T)
Photon Detection Efficiency	$\geq 20\%$	$\geq 20\%$

Microchannel plate photomultipliers (MCP-PMTs) from commercial vendors such as Photonis and Hamamatsu have been shown to have extraordinarily good timing and position resolution as well as high magnetic field tolerance [6–8], but are generally far too expensive for widespread use, since the current cost is, for instance, about \$12K for one $53 \times 53\,\text{mm}^2$ MCP-PMT from Photonis. The recently commercialized Large Area Picosecond Photo-Detector (LAPPD) [9–11] provides a promising cost-effective MCP-PMT for the EIC DIRC and RICH sub-systems. By creating activated micro-channel plates using the atomic layer deposition (ALD) technique to apply resistive and secondary emissive layers on large-area glass capillary substrate, the cost of LAPPD is expected to be at least an order of magnitude lower per active area than that of traditional MCP-PMTs. Optimization of the LAPPD design for high magnetic-field tolerance, precision timing resolution and pixelated readout was performed at Argonne National Laboratory (ANL) with $6 \times 6\,\text{cm}^2$ size format. This effort aims to adapt the LAPPDs to the EIC-PID requirements with optimized design parameters integrated into the low-cost LAPPD production.

2 Argonne MCP-PMT design for EIC-PID

The standard LAPPD employs a borosilicate float glass hermetic package with two ALD functionalized MCPs placed at Chevron configuration for electron multiplication and silk-screened silver
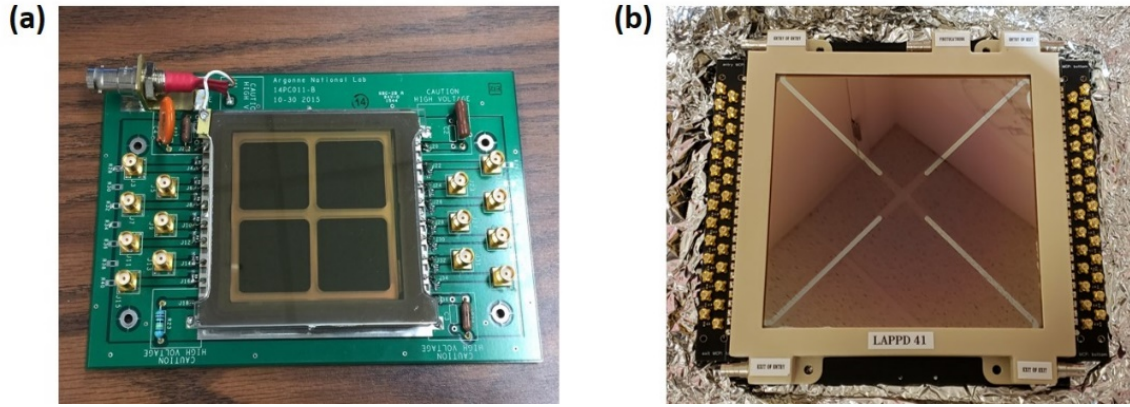
Figure 1. One possible configuration designed at ANL for a pixelated MCP-PMT with all glass/fused silica package for Cherenkov imaging application.

striplines on the glass base for signal pickup. Unfortunately, the stripline signal readout is not suitable for Cherenkov imaging applications and thus needs to be replaced with a pixelated readout. In addition, the MCP pore size and internal configuration need to be optimized for high magnetic field tolerance (above 1.5 Tesla) and precision timing root-mean-square (RMS) resolution ($\sim 100\,\mathrm{ps}$).

Figure 1 shows one possible configuration designed at ANL for a pixelated MCP-PMT with all glass/fused silica package for Cherenkov imaging application. Several optimizations are proposed in the Argonne MCP-PMT design: (a) Fused silica window is used here to replace the borosilicate float glass window. The fused silica extends the MCP-PMT sensitivity down to $\sim 180\,\mathrm{nm}$ with bialkali photocathodes, increasing the number of photoelectrons generated from Cherenkov light, since Cherenkov emission is strongest in the ultra-violet range. (b) newly developed $10\,\mu\mathrm{m}$ pore size MCPs are used to replace the $20\,\mu\mathrm{m}$ pore size MCPs. The smaller pore size MCPs provide higher magnetic field tolerance and more precise timing resolution of the MCP-PMT. (c) The internal geometry is optimized here with smaller spacing lengths between photocathode, MCPs, and anode. The reduced spacing further improves the magnetic field tolerance and timing resolution of the MCP-PMT. (d) A capacitively coupled electronic readout scheme through glass/fused silica is applied here to replace the stripline readout. The glass/fused silica base is coated with a resistive anode, and users may then design their own printed circuit board (PCB), customized to their requirements (pixel size, pitch distance etc...) and placed on the external side of the glass/fused silica base to pick up the fast MCP-PMT signals through capacitive coupling. This is similar to the design in the multi-gap resistive plate chamber (mRPC), where electron clusters generated in the gas gaps are collected on the internal resistive anode and fast signals are picked up on the printed circuit board (PCB) outside the active field regions of the detector.

The Argonne MCP-PMTs are small form-factor LAPPDs, they employ the same ALD functionalized MCPs and share the same design as that of the LAPPDs. Figure 2 shows photos of the Argonne $6 \times 6\,\mathrm{cm}^2$ MCP-PMT and Incom $20 \times 20\,\mathrm{cm}^2$ LAPPD. Design modification for desired requirement are perfromed on the smaller size Argonne MCP-PMTs, and the optimized parameters could be easily transferred to LAPPD production for industrial implementation.

Figure 2. Images of Argonne MCP-PMT and LAPPD: (a) Argonne $6 \times 6\,\text{cm}^2$ MCP-PMT for research and development; (b) commercialized Incom $20 \times 20\,\text{cm}^2$ LAPPD.

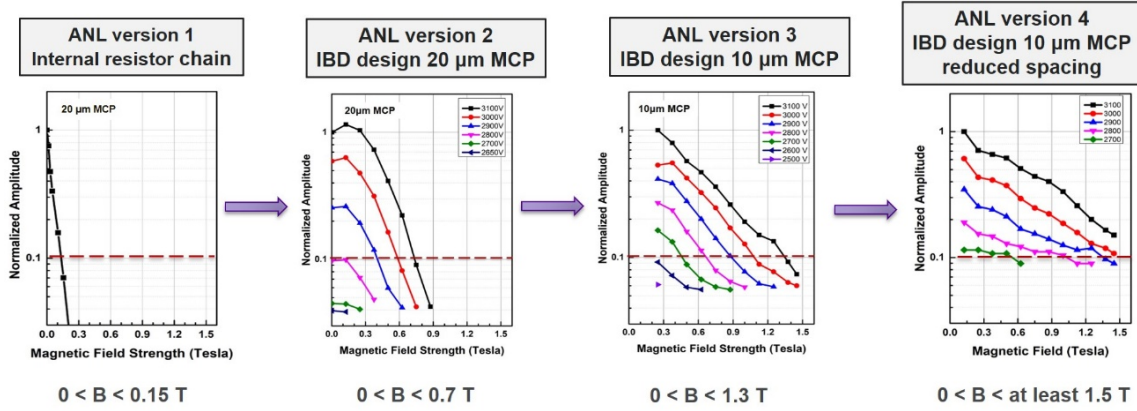## 3   Magnetic field tolerance and precision timing

The MCP pore size and internal spacing lengths determine the distance that photoelectrons travel inside the MCP-PMT, and thus strongly affect its magnetic field tolerance and precision timing performance. Four MCP-PMTs with different pore size MCPs and internal spacing length parameters were fabricated at Argonne to systematically explore the internal geometry effect. Version 1, had an early internal resistor chain design with $20\,\mu\text{m}$ pore size MCPs and relies on internal glass spacers with resistive coating to control the high voltage (HV) distribution. Version 2, had an independently biased design again with $20\,\mu\text{m}$ pore size MCPs and applies non-coated glass spacers but has five HV feedthroughs, providing the advantage of tuning the MCP HVs independently for best performance. Version 3 had an independently biased design with $10\,\mu\text{m}$ pore size MCPs, a similar internal design as version 2 but with a smaller pore size MCPs. Finally, version 4 had an independently biased design as version 2 and 3 but with $10\,\mu\text{m}$ pore size MCPs and reduced spacing lengths with thinner glass spacers to reduce the photoelectron travel distance.

3.1   Magnetic field tolerance

The magnetic field tolerance of the Argonne fabricated MCP-PMTs was characterized on a system [12] featuring a decommissioned superconducting magnet from a magnetic resonance imaging (MRI) scanner with a tunable magnetic field strength of up to 4 Tesla. A non-magnetic, light-tight dark box was made to accommodate the MCP-PMT. A pulsed 405 nm light-emitting diode (LED) was used as the light source and was introduced to the dark box through an optical fiber. High voltages were applied to the MCPs from a power supply with continuous voltage control, and signals from the striplines were read out through the CAEN DT5742 desktop digitizer.

Figure 3 shows the continuous improvement of the magnetic field tolerance of the MCP-PMTs as the HV internal bias design (IBD), MCP pore size and internal geometry were optimized in different versions. The relative decrease trend of the signal amplitude was plotted as a function of the magnetic field strength, and the 10% value relative to the maximum signal was chosen to indicate the magnetic field tolerance of the MCP-PMT. During the device fabrication, after the baking and scrubbing processes, the resistance of ALD functionalized MCP changes. In version 1 device the
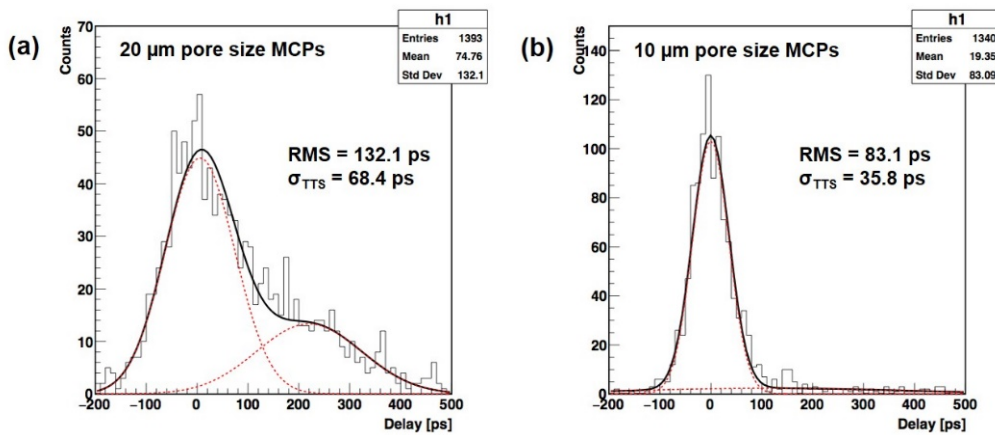
Figure 3. Improvement of magnetic field tolerance for different versions of the Argonne MCP-PMTs, the magnetic field tolerance was improved an order of magnitude from 0.15 T to over 1.5 T.

change is largely mismatched resistances of the MCPs and the spacers, making it impossible to have both MCPs operating at the optimal bias HV. However, with the independently biased design (version 2 device), both MCPs can be tuned to operate at the optimal HV, resulting in a significant improvement of MCP-PMT magnetic field tolerance from 0.15 T to 0.7 T. With a 10 μm pore size MCPs, the magnetic field tolerance of the MCP-PMT was further improved to 1.3 T and eventually to be over 1.5 T by reducing the MCP-PMT internal spacing lengths. Further improvement of the MCP-PMT magnetic field tolerance is possible with 6 μm pore size MCPs, which are presently under development at Incom, Inc [13].

3.2 Precision timing

The use of smaller pore size MCPs reduces the travel distance of photoelectrons inside the MCP-PMT, resulting in improved timing resolution of the devices. Figure 4 shows the transit time spread (TTS) [14] of two Argonne MCP-PMTs with 20 μm pore size MCPs (version 2 device) and new

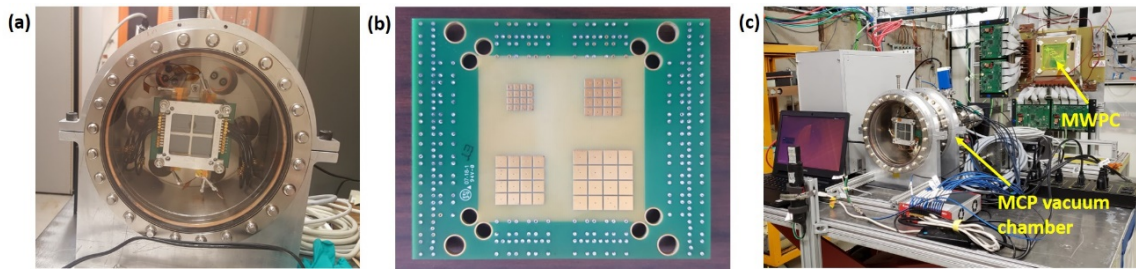**Figure 4**. Transit time spread of two Argonne MCP-PMTs within a delay time window of −200 ps to 500 ps: (a) version 2 device with 20 μm pore size MCPs; (b) version 3 device with new 10 μm pore size MCPs.

10 μm pore size MCPs (version 3 device). The root-mean-square (RMS) value of the transit time spread of the MCP-PMTs within a delay time window of -200 ps to 500 ps, which is a more practical precision timing parameter of the MCP-PMT adopted by the PANDA DIRC group [7], are 132 ps and 83 ps, respectively. The below 100 ps RMS TTS timing resolution within the delay window would allow for a correction of the chromatic dispersion and significantly improve the proposed high-performance DIRC resolution.

4 Pixelated readout

A highly pixelated readout scheme is essential for Cherenkov imaging related applications. This is especially true for collider physics experiments, due to the limited space of the compact detector designs, requiring a fine pixel size of 2–3 mm level. The high occupancy issue also requires pixel readout scheme to detect the rather large number of Cherenkov photons in a DIRC.

An MCP vacuum chamber as shown in figure 5(a) was designed to be a flexible set up to validate pixel readout schemes without actually manufacturing a sealed MCP-PMT. The chamber is dynamically pumped with a turbopump to maintain a vacuum of 10^{-7} torr. The chamber is fixed on an aluminum holder with a flat base to ensure stable placement on a flat surface, compatible with the Fermilab test beam facility (FTBF) platform. Inside the chamber is the MCP stack and electronic readout scheme to mimic the MCP-PMT operation. The high voltages are provided to the MCPs via SHV (safe high voltage) feedthroughs, and the signals are led out from SMA (Sub Miniature Version A) feedthroughs. Figure 5(c) shows the vacuum chamber installed on the platform of FTBF. In this vacuum setup, since there is no high QE photocathode, signals are produced via (beam particle direct) ionization in the MCPs which then initiate the secondary electron avalanche. A 120-GeV proton beam was used in our tests to generate primary electrons in the MCPs. The signals were picked up with 4×4 pixel arrays of 2 mm, 3 mm, 4 mm and 5 mm sizes as shown in figure 5(b) following different readout schemes. Several multi-wire proportional chambers (MWPC) with 1 mm pitch were used as tracking stations along the beam.
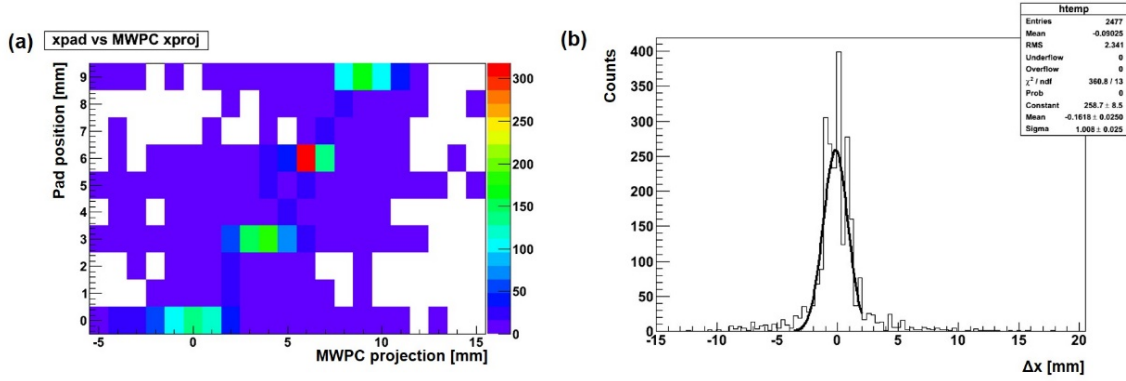

Figure 5. (a) MCP vacuum chamber with an MCP stack-up and PCB board installed; (b) a pixelated PCB board with 4×4 pixel arrays of 2 mm, 3 mm, 4 mm and 5 mm sizes; (c) the MCP vacuum chamber installed on the platform of FTBF with MWPC as tracking stations.

4.1 Direct signal pickup

The performance of the pixel array was tested by directly picking up the signals from the MCP stack. Following the proton beam direction, the MCP stack includes a top glass with thin aluminum

photocathode, two Chevron MCPs and the pixelated PCB board. The proton beam was aligned with the center of a pixel array, and the electron avalanches from the MCP stack were directly collected by the pixel array. The MWPC tracking projection was correlated with the pixel location (X-, Y-axis), and the spread of the difference between the pixel location and the MWPC projection was fitted to obtain the position resolution of the pixels.

Figure 6. (a) Correlation between the X-axis of a $3 \times 3\,\text{mm}^2$ pixel and the MWPC projection for direct signal pickup scheme; (b) fitting of the spread of the position difference between pixel position and MWPC projection for position resolution.

Figure 6 shows an example of the correlation between the X-axis of a $3\,\text{mm} \times 3\,\text{mm}$ pixel and the MWPC projection, the spread fitting gives a position resolution of 1.01 mm which agrees with the expected position resolution of 0.87 mm with a single pixel hit ($\sigma_{\text{expected}} = \frac{\text{pixelsize}}{\sqrt{12}}$). The measured position resolutions along the X- and Y-axis with different pixel sizes are listed in table 2, the experimental results are close to the expected single pixel hit position resolution for all pixel sizes, which are also listed in table 2.

Table 2. Position resolution along X- and Y-axis of pixels with different sizes and readout schemes.

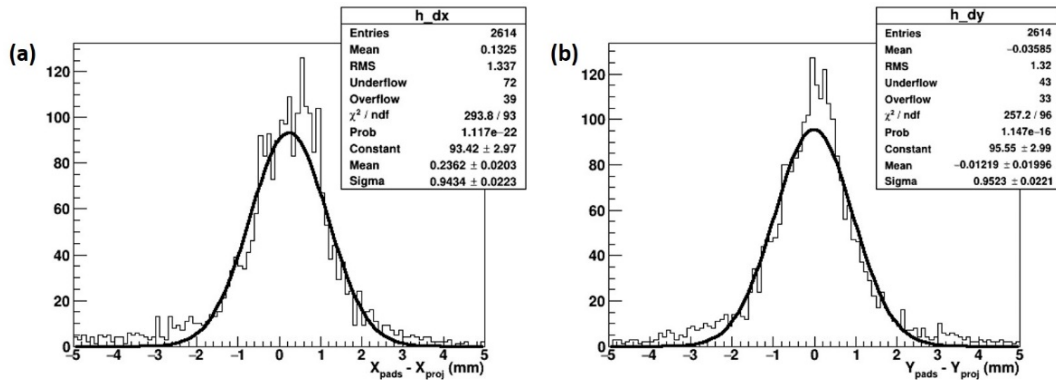| Readout scheme		$2 \times 2\,\text{mm}^2$	$3 \times 3\,\text{mm}^2$	$4 \times 4\,\text{mm}^2$	$5 \times 5\,\text{mm}^2$
Direct signal pickup	σ_X (mm)	-	1.01	1.11	-
	σ_Y (mm)	0.73	0.93	1.43	-
	σ_{expected} (mm)	0.58	0.87	1.15	-
Capacitively coupled	σ_X (mm)	1.4	0.94	0.81	1.1
signal pickup	σ_Y (mm)	1.7	0.95	0.76	0.97

4.2 Capacitively coupled signal pickup

To manufacture a functional MCP-PMT with pixelated readout, a gas-tight anode base is required to ensure a high vacuum inside the MCP-PMT. Commercial MCP-PMTs apply high temperature co-fired ceramic (HTCC) for hermetic packaging and direct signal pickup, given its desirable electrical properties, high mechanical strength and good thermal conductivity. However, the HTCC anode dramatically increased the photodetector cost, making them unaffordable for large instruments.

An elegant solution may be to use a capacitively coupled readout as described in section 2. In this solution, instead of an internal pixel layer with signal feedthroughs, a resistive anode is created at the bottom of the MCP stack. The signals can then be capacitively coupled to a PCB with pixels on the outside of the sealed MCP-PMT. This allows the user to optimize the pixel design for the specific application. Another advantage is that with capacitive coupling, signals will be shared among pixels, allowing for interpolation of the position and therefore potentially improving the position resolution beyond the pitch-width $/\sqrt{12}$ that is standard for a single pixel hit. This could allow for larger pad sizes while still achieving the desired resolution, which reduces the channel count and saves on cost and power. However, a disadvantage with charge sharing is that the cluster size increases, and thus one has to be careful of occupancy effects. This is a concern for the DIRC, and less of a concern for the mRICH and gaseous RICH detectors.

A capacitively coupled MCP stack was installed into the MCP vacuum system, and placed in the proton beam at FTBF. Comparing to the direct signal pickup stack, the capacitively coupled MCP stack included a glass anode base with resistive coating between the MCPs and PCB board. Here, the hit position on the MCP stack was derived using a simple mean of the charge amplitudes in each pixel. MWPCs were used to track protons and the track fit was projected onto the MCP stack to determine the position resolution of a capacitively coupled readout. The distribution of the difference between the track projection and the hit location determined from the pixels with $3 \times 3\,\text{mm}^2$ size is shown in figure 7 for both the X and Y directions, exhibiting a position resolution of $\sigma_X = 0.94\,\text{mm}$ and $\sigma_Y = 0.95\,\text{mm}$. Table 2 lists σ_X and σ_Y from tests with other pixel sizes. The sigmas are all around 1 mm, and generally get smaller with smaller pixel sizes. The increase in sigma for the $2 \times 2\,\text{mm}^2$ pixel is due to losses of the signal at the edge of the pixels, since the $2 \times 2\,\text{mm}^2$ pixel array only covers $8 \times 8\,\text{mm}^2$ (the beam spot from the 120 GeV protons is itself around 3–4 mm wide in the horizontal direction). The MWPCs consist of four X-Y hodoscope planes, with 1 mm pitch wires in each plane. Our preliminary estimates of the projection resolution using the MWPC is about 0.6 mm, but this has not been accounted for in table 2 pending further refinements in our analysis. The results show that a capacitive coupling design through glass enables pixelated readout for the LAPPD MCP-PMTs, and can achieve position resolutions that are better than with direct pixel readout due to the charge sharing effect, at large pixel size. When taking

Figure 7. Fitting of the distribution of the difference between the hit location of a 3 mm × 3 mm pixel and the MWPC track projection for capacitively coupled readout scheme: (a) X-axis; (b) Y-axis.

into consideration the cluster sizes from charge sharing using this scheme, and estimates of the occupancy for the RICH, mRICH, and DIRC detectors at the EIC, there should be no problem with overlapping clusters for the lower occupancies in the RICH and mRICH detectors, but there may be a problem for the DIRC. This requires further study in simulation and also in optimizing the cluster size of a capacitively coupled MCP-PMT.

5 Conclusion

We have described an optimized low-cost all glass/fused silica MCP-PMT design applicable to Cherenkov imaging sub-systems for EIC particle identification. The magnetic field tolerance and precision timing properties were significantly improved by applying newly developed 10 μm pore size MCPs and reducing the internal spacing lengths. We achieved a magnetic field tolerance of over 1.5 Tesla and an RMS TTS time resolution of below 100 ps. Highly pixelated readout based on capacitive coupling through glass was also explored with MCP stack and readout board in an MCP vacuum chamber at the Fermilab test beam facility. We demonstrated pixelated readout with capacitive coupling design through glass for the LAPPD MCP-PMTs, and achieved position resolutions of less than 1 mm, these are better than with direct pixel readout due to the charge sharing effect at large pixel size. With the demonstration of the magnetic field tolerance, precision timing and pixelated readout, we are fabricating sealed Argonne $6 \times 6 \, cm^2$ MCP-PMTs with these parameters integrated. Since the Argonne MCP-PMT shares the same manufacturing details with the commercial LAPPD, knowledge, techniques and optimized design parameters are transferrable to industrial partners for low-cost LAPPDs production to achieve the demonstrated performances.

References

[1] A. Accardi et al., *Electron ion collider: The next QCD frontier*, *Eur. Phys. J.* **A 52** (2016) 268.

[2] A. Aprahamian et al., *Reaching for the horizon: The 2015 long range plan for nuclear science* (2015).

[3] National Academies of Sciences, Engineering, and Medicine, *An Assessment of U.S.-Based Electron-Ion Collider Science*, The National Academies Press, Washington, D.C., U.S.A. (2018) [doi:10.17226/25171].

[4] X. He, *RICH detector development for the Electron-Ion Collider experiments*, *Nucl. Instrum. Meth. A 952* (2020) 162051.

[5] T. Ullrich, *The Electron-Ion Collider Detector Needs*, presented at *New Technologies for Discovery IV: The 2018 CPAD Instrumentation Frontier Workshop*, Providence, RI, U.S.A., 9–11 December 2018.

[6] A. Lehmann et al., *Performance studies of microchannel plate PMTs in high magnetic fields*, *Nucl. Instrum. Meth. A 595* (2008) 173.

[7] A. Lehmann et al., *Recent progress with microchannel-plate PMTs*, *Nucl. Instrum. Meth. A 952* (2020) 161821.

[8] V.A. Grigoryev et al., *Study of the Planacon XP85012 photomultiplier characteristics for its use in a Cherenkov detector*, *J. Phys. Conf. Ser. 675* (2016) 042016.

[9] M.J. Minot et al., *Pilot production & commercialization of LAPPD™*, *Nucl. Instrum. Meth. A 787* (2015) 78.

[10] M.J. Minot et al., *Large Area Picosecond Photodetector (LAPPD™) — Pilot production and development status*, *Nucl. Instrum. Meth. A 936* (2019) 527.

[11] A.V. Lyashenko et al., *Performance of Large Area Picosecond Photo-Detectors (LAPPD™)*, *Nucl. Instrum. Meth. A 958* (2019) 162834.

[12] M. Hattawy et al., *Characteristics of precision timing MCP-PMTs in magnetic fields*, *Nucl. Instrum. Meth. A 929* (2019) 84.

[13] C. Ertley et al., *Performance studies of atomic layer deposited microchannel plate electron multipliers*, *Nucl. Instrum. Meth. A 912* (2018) 75.

[14] J. Xie et al., *Fast-timing microchannel plate photodetectors: Design, fabrication, and characterization*, *Rev. Sci. Instrum. 90* (2019) 043109.